Applied Clay Science 194 (2020) 105698

Contents lists available at ScienceDirect

Applied Clay Science

journal homepage: www.elsevier.com/locate/clay

Note

Crack behaviour and mechanical properties of thermally treated kaolin based ceramics: The influence of pore generating agents

David O. Obada[a,g,**], David Dodoo-Arhin[b,*], Muhammad Dauda[a], Fatai O. Anafi[a,g], Abdulkarim S. Ahmed[c,g], Olusegun A. Ajayi[c], Stefan Csaki[d,e], Naresh D. Bansod[f], Idris I. Kirim[a], Omeiza J. Momoh[c]

[a] Department of Mechanical Engineering, Ahmadu Bello University, Zaria, Nigeria
[b] Department of Materials Science and Engineering, University of Ghana, Legon, Ghana
[c] Department of Chemical Engineering, Ahmadu Bello University, Zaria, Nigeria
[d] Charles University, Faculty of Mathematics and Physics, Ke Karlovu 5, 121 16 Prague, Czech Republic
[e] Institute of Plasma Physics, The Czech Academy of Sciences, Czech Republic
[f] Department of Chemistry, Mahatma Gandhi Arts, Science and Late N.P. Commerce College, Armori (M.S.) 441208, India
[g] Africa Center of Excellence on New Pedagogies in Engineering Education, Ahmadu Bello University, Zaria, Nigeria

ARTICLE INFO

Keywords:
Ceramic supports
Mechanical integrity
Microstructure
Fracture
Crack propagation

ABSTRACT

In this study, the crack behaviour of porous kaolin based ceramics was experimentally investigated. The samples (ceramic bodies) were fabricated with the inclusion of pore formers in determined proportions and subjected to heat treatment. Next, the apparent porosity of the samples was measured using the water immersion method. The values confirmed the increased porosity (up to 47%) for the samples with embedded pores. We speculated that the open pores on the surface of the samples which were quite evident, especially with styrofoam as pore formers, may also have penetrated through, hence the enhanced porosity values for the samples. Acoustic emission (AE) activity which reveals the formation of microcracks in the ceramics due to the different thermal expansion coefficients in the cooling stage was recorded for the samples. The first signals of AE counts appeared at 800 °C, where the compressive stresses between the different phases (particles with different coefficients of thermal expansion) led to an appearance of microcracks. By introducing porosity to the samples, the AE signals were less pronounced. This was evident for the samples with sawdust as pore formers, and it was inferred that in this sample, microcracking was suppressed. As a validation protocol for AE measurements, mechanical measurements on the produced samples were conducted through the indentation technique to obtain the fracture toughness of the samples. The results conformed to the observation made during AE measurements. The samples embedded with sawdust as porogens produced the highest fracture toughness of 4.77 MPa.m$^{1/2}$ by reason of the suppression of microcracking after heat treatment.

1. Introduction

Simply by reason of their intrinsic properties, porous ceramics have gained significant attention for many industrial applications such as filters (Dey et al., 2013), catalyst support (Danwittayakul and Dutta, 2014), thermal insulators (Fukushima and Yoshizawa, 2016), and heat exchangers (Villanueva and de Mello, 2015) due to their specific properties like large surface area, high permeability, thermal stability and low thermal conductivity (Obada et al., 2016a; Obada et al., 2016b). One of the simple procedures to fabricate porous ceramics is by using pore-forming agents (Rice, 1998; Scheffler and Colombo, 2006; Studart et al., 2006) which are introduced during the fabrication process and burn out completely during sintering. In addition, high temperature sintering has the tendency to sufficiently increase the strength while reducing the open porosity to some extent. Nonetheless, the pores generated in this way are usually believed to degrade the mechanical integrity (Ohji and Fukushima, 2012). Hence, it is important to elucidate the degradation tendency of, for instance, fracture behaviour of ceramic membranes which are expected to resist large pressure gradients that are induced during their practical applications (Biesheuvel and Verweij, 1999). In addition to using porogens, further fabrication routes involve solid state sintering and chemical methods (Mei et al.,

* Corresponding author at: Department of Materials Science and Engineering, University of Ghana, Legon, Ghana.
** Corresponding author at: Department of Mechanical Engineering, Ahmadu Bello University, Zaria, Nigeria.
E-mail addresses: doobada@abu.edu.ng (D.O. Obada), ddodoo-arhin@ug.edu.gh (D. Dodoo-Arhin).

https://doi.org/10.1016/j.clay.2020.105698
Received 11 January 2020; Received in revised form 11 May 2020; Accepted 26 May 2020
Available online 05 June 2020
0169-1317/

2000; Azin et al., 2005; Gonzalez-Velasco et al., 2005; Kouras et al., 2017). Assessing these methods, solid state sintering method has been used extensively by reason of its simplicity. However, this protocol only suits very high temperatures which consequently cause the appearance of cracks and loss in mechanical integrity.

The relationship between the starting materials and advanced fabrication processes of ceramic substrates has led to a considerable progress in this area of scientific importance and have provided a new class of high performance inorganic ceramic membranes which combines well defined porosity, mechanical strength, separation efficiency and selectivity, etc. (Lenza and Vasconcelos, 2000; Romanos et al., 2001; Van Gestel et al., 2002; Chang et al., 2014; Obada et al., 2016c; Obada et al., 2017a; Obada et al., 2017b; Obada et al., 2017c). The mechanical integrity of these membranes has also been a subject of intense interest (Zhu et al., 2015; Obada et al., 2017a; Zuo et al., 2017; Aziz et al., 2019; Wang et al., 2019; Yang et al., 2019).

Despite the very broad interest in ceramic membranes at the moment, the fracture behaviour of the membranes during cooling have received limited attention especially when it relates to porous membranes which originally have had their mechanical properties degraded by the embedded pores. Fracture toughness is a property that gives information about the resistance of membranes to crack growth and fracture, and is another important property of ceramics membranes which is hugely considered for design application (Green, 1998). Fracture typically occurs when the stress applied is enough to break the atomic bonds inherent in the solid (Anderson and Anderson, 2005; Scholz, 2002).

Some research efforts on the mechanical measurement of porous ceramics mainly focused on the influence of the inherent microstructure on mechanical integrity (Chakrabarti et al., 1994; Jang et al., 2010) and heat treatment (Kim et al., 1999; Wilhelm and Wruss, 2000; Obada et al., 2017a) during the ceramic processing. There is a clear need to reveal preliminary findings on the crack propagation mechanisms and fracture toughness of porous ceramics. Hence this study is divided into two portions:

1. To verify the effect of pore generating agents on the crack propagation and fracture behaviour of thermally treated ceramic bodies, especially during cooling.
2. As a validation protocol to the current study on crack propagation of porous ceramics, since the appearance of cracks may result in the reduction of mechanical properties, mechanical properties of porous thermally treated ceramic pellets using the same pore formers was reported.

2. Experimental

2.1. Materials and processing

Kaolin obtained from Kankara and Kibi deposits in Nigeria and Ghana were used after a beneficiation process as elaborated in a previous study (Obada et al., 2016a). Sawdust and styrofoam were used as pore generators with a broad range of particle sizes: $^{>}$1 nm–8000 nm (Obada et al., 2017b). The processed pore formers were mixed singly with kaolin in different ratios by volume (see Table 1). The elemental composition of kaolin (Kankara and Kibi kaolin) used for the samples fabrication revealed that the kaolin used were composed mainly of aluminosilicates while the structure of the base kaolin (Kankara kaolin) suggested that the clay consists of mainly kaolinite, quartz, and illite. Kibi kaolin was practically noticed to be more plastic comparatively and was used as a plasticizer.

Table 1
Composition of the Batch formulation.

Sample code.	Kankara Kaolin (g)	Kibi Kaolin-Plasticizer (g)	Saw dust (% vol.)	Styrofoam (% vol.)
A	70	20		10
B	70	20	10	–
C	80	20	–	–

2.2. XRD analysis of kaolin and pore formers

To investigate the structure and phases present in the raw materials, X-ray powder diffraction (XRD) patterns were collected on an Empyrean diffractometer operating a copper tube (λ = 1.5418A) generated at a voltage of 40 kV and a current of 30 mA. The goniometer was set at a scan rate of 0.033°/s over a 2θ range of 5-80° for kaolin (considering the existence of illite) and 10-80° for the pore generators.

2.3. Fabrication of the samples

The formulation as shown in Table 1 were mixed with water, kneaded and filled into a mould to ensure dimensional accuracy. The prepared samples before sintering were dried in open air at room temperature for three days and further dried in an oven at 100 °C. Next, sintering at 1150 °C for 2 h at 5 °C/min was conducted on the samples (25 mm × 25 mm × 25 mm). Sample prepared with styrofoam as pore former was denoted as sample A, sample prepared with sawdust as pore fore was denoted as sample B, while sample prepared with kaolin alone was denoted as sample C.

2.4. Morphological studies

The morphology of the samples was studied on a FEI Xl-30 scanning electron microscope (SEM) operated at 15 kV. Field emission scanning electron microscope (FESEM) images of the samples were conducted using a Hitachi S-4800 FESEM operated at 5 kV to visualize topographic details on the surface of the samples as a complement to SEM images. The samples for both microscopic observations were gold sputtered with an ultrathin (5 nm) coating of gold under vacuum for 3 min.

2.5. Measurement of the apparent porosity

The apparent porosity was calculated using Eq. (1)

$$Apparent\ porosity = \left(\frac{W - D}{W - S}\right) \times 100 \quad (1)$$

where: W = Weight of immersed sample when suspended in air; D = Weight of sintered sample and S = Weight of sintered sample suspended in water.

2.6. Acoustic emission tests

Acoustic emission equipment was used to experimentally investigate the crack modes in the samples during the cooling stage using the DAKEL-XEDO-3 AE system. A piezoelectric AE sensor MST8S (Ø 3 mm, flat response in the frequency interval from 100 up to 600 kHz) was mounted to one end of an alumina rod (Ø 3 mm, length 20 cm), which served as a waveguide. The AE activity was collected as counts per second (count rate) and plotted against the measured temperature. More details on the experimental protocol have been discussed in a study carried out by Amlabu et al. (2019). The protocol was conducted at a heating rate of 10 °C/min up to 1200 °C with a dwell time of 4 h and the furnace was cooled at 5 °C/min.

2.7. Mechanical testing

The formulation (Table 1) in powdery form was cold pressed with a pressure of 500 Pa into square shaped pellets (25 mm × 25 mm × 25 mm). Next, the pellets were subjected to heat

treatment at 1000 °C for 2 h in a muffle furnace at a heating and cooling rate of 5 °C/min and allowed to furnace cool. The mechanical properties measurements conducted for the prepared pellets were hardness, compression strength, Young modulus and fracture toughness.

2.7.1. Hardness testing

The micro hardness (Hv) of the sintered samples was determined via the Vickers indentation with a micro hardness tester (HV-1000). The pellets were subjected to an applied load of 300 g for a dwell time of 10 s. A total of 5 indentations were made and the resulting hardness values were averaged.

2.7.2. Compressive strength evaluation

The compressive strength of the prepared pellets was determined using a universal testing machine (UTM), equipped with a 5 kN load cell.

2.7.3. Fracture toughness testing

The fracture toughness, K_{IC} in MPa was calculated from hardness test parameters according to Eq. (2):

$$K_{IC} = 0.016\left(\frac{E}{Hv}\right)^{0.5}\frac{P}{C^{1.5}} \quad (2)$$

where: Hv = micro hardness value,

E = Young modulus,

P = applied load,

C = is the crack length. The other details of mechanical evaluations are reported elsewhere (Obada et al., 2020).

3. Results and discussion

The pronounced reflections (Fig. 1) at 2θ = 12.36°, 24.90°, 35.98°, 38.46°, 45.66°, 55.12° and 62.34° were identified as belonging to kaolinite, in agreement with reports elsewhere (Nandi et al., 2008; Nandi et al., 2009). On the XRD spectrum of sawdust (Fig. 1), the reflections of the crystalline plane were observed at 2θ ≈ 22°, and lowest value of amorphous region was found to be at 2θ ≈ 18° which corresponds to (101) and (002) lattice planes of cellulose. A tiny reflection was also observed at 2θ° =34.7°, attributing to (400) plane of crystalline cellulose. Considering styrofoam, a broad reflection was noticed at ~20° indicating the amorphous nature of polystyrene (Ismail et al., 2017).

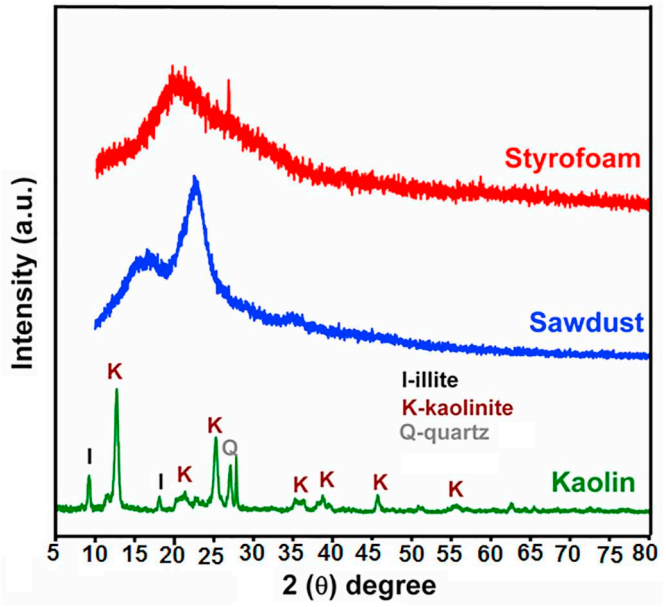

Fig. 1. X –ray diffraction patterns of raw materials.

The morphology of the prepared samples with kaolin and 10 vol% of pore formers fired at 1150 °C for a holding time of 2 h is shown in Fig. 2. On the images, some intervening pore walls can be seen on images: a,b and, a'b' which is due to the fraction of pore formers embedded. Images c and c' show very limited pores embedded because no pore formers were incorporated. Typically, the open pores embedded in a ceramic membrane are characterized by the intergranular packing influence of the starting raw materials which is mainly dependent on the surface topography and the distribution of the particle sizes. Hence, open pores are more noticeable on samples with styrofoam as compared with sawdust as porogens. Open porosity was observed to increase relatively to the reference sample (0% pore formers) as well, which indicates that the addition of the pore formers is quite responsible in enhancing the porosity.

The apparent porosity of the samples was further evaluated by water immersion method (Table 2). Following up on the SEM images, it is possible to speculate that the open pores on the surface of the samples which were quite evident with styrofoam as pore formers may also have penetrated through the samples, hence the enhanced porosity value for sample A.

Fig. 3 presents the recorded AE activity during the cooling phase in terms of counts per second (cps). The first signals appeared at 800 °C, where the compressive stresses led to a formation of microcracks. These stresses originated from the different thermal expansion coefficients of the different phases. The beginning of the microcrack formation was observed at the same temperature in all samples, thus being independent on the porosity. In the vicinity of the temperature of ~576 °C, where the $\beta \rightarrow \alpha$ transformation of quartz takes place, a relaxation of stresses led to a decrease in the AE activity. This feature was observed in all samples. As the temperature further decreased, a formation of circumferential cracks around the quartz grains led to the recorded AE activity (Knapek et al., 2016). The increased porosity led to a decreasing AE activity which was more evident in the sawdust pore induced sample, suggesting that the porosity suppressed the crack formation. The AE activity is observed during the whole cooling range, suggesting that the microcracking occurs over the whole temperature interval.

Fig. 4 presents the FESEM images of the fractured surfaces with inherent cracks. The microstructure reveals that more cracks were observed on the surface of the sample C (sample prepared with kaolin only). Cracks noticed for the pore embedded samples were as a result of the burn-out of the porogens and possible cracks between the walls of the voids and the thermal expansion gradient of the porogens during the heating process. The large cracks observed on the samples can contribute significantly to the gradient in their mechanical properties. Stemming from the AE results and relating same to the FESEM images, the increased porosity suggests that the porosity suppressed the crack formation.

The large particles observed in the FESEM images is as a result of the random structure of the kaolin powders which can induce different shapes and sizes and has the tendency to change orientation due to the preparation protocol. Particle agglomeration as observed in Fig. 4 can be attributed to the smaller particle sizes of kaolin and smaller particles tend to agglomerate more easily. These small particles formed a cluster of agglomerated particles and large particle sizes of kaolin were obtained. These assertions are in line with studies carried out by Masuda et al. (2006) and Capes (2013). It is not clear if the presence of large particles influenced the appearance of cracks, however, that could be investigated in more detail.

Based on our knowledge, the propagation of cracks has been noticed to start near macro pores embedded in the samples and at different locations inside the samples (see SEM and FESEM images). Then, these cracks propagate especially by linking macro-pores through their clusters. Regularly spaced macro pores were observed for samples with sawdust as pore formers which should lead to improved fracture strength. These observations are in line with the hypothesis developed

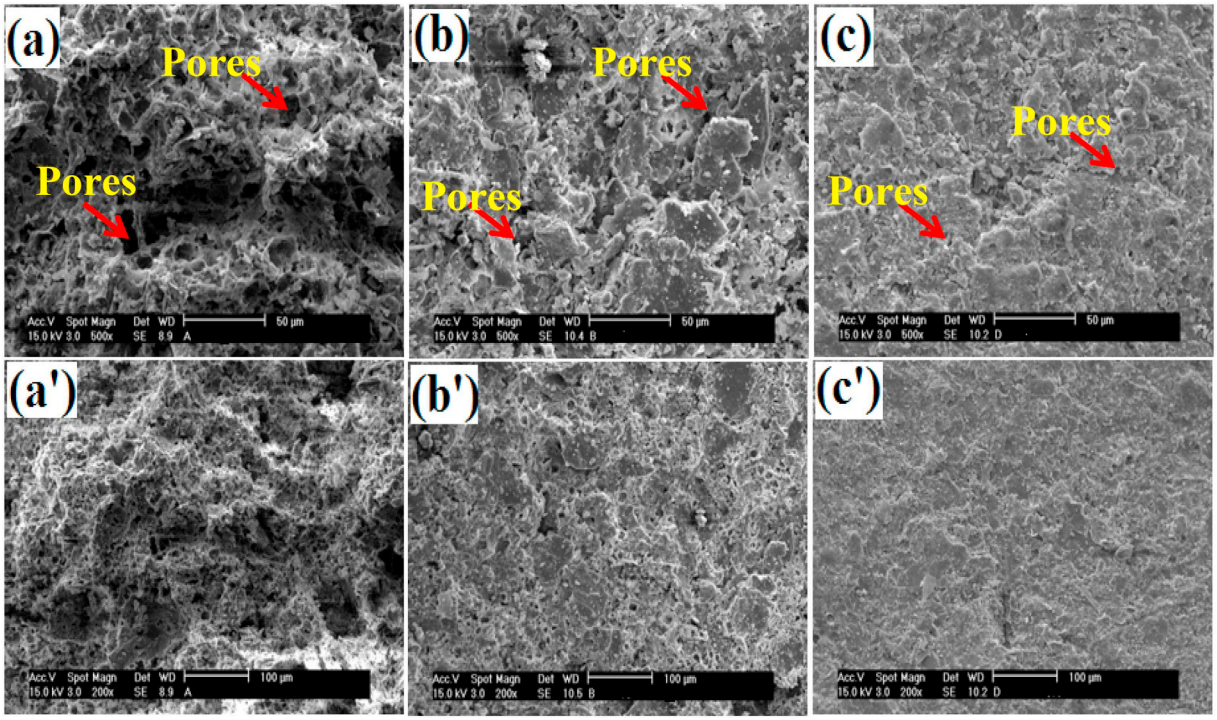

Fig. 2. Scanning electron microscopy images of (a) Kaolin + Styrofoam; (b)Kaolin + Sawdust; (c) Kaolin - at higher magnification (500×) and (a′) Kaolin + Styrofoam; (b′) Kaolin + Styrofoam (c′) Kaolin- at lower magnification (200×).

Table 2
Porosities of the samples.

Sample code	% P_a	% P_b	% P_c	% P_d	% P_e	% P_{avg}	SD
A (styrofoam 10%)	47.13	47.01	47.12	47.10	47.11	47.09	0.05
B (sawdust 10%)	41.30	41.27	41.21	41.25	41.21	41.24	0.03
C (Kaolin only)	28.63	28.61	28.63	28.60	28.61	28.61	0.01

% $P_{a\text{-}e}$ = Percentage porosities of each of the 5 samples.
% P_{avg} = Average percentage porosities of each of the 5 samples.
SD = Standard Deviation.

by different authors (Cannillo et al., 2004; Tancret et al., 2006) about the influence of the clusters of macro pores.

Mechanical measurement data are presented in Fig. 5. Hardness (Hv) of the samples were observed to increase from 0.51 GPa to around 0.70 GPa as we go from sample with styrofoam to sample with sawdust, meaning the sample without pore former (kaolin alone) was measured as having hardness value of 0.68 GPa, which was a value between the values measured for the pore induced samples. The gradient in mechanical properties for these samples, especially for the sample with sawdust as pore formers with the highest hardness value can be attributed to the fraction of porosity which is able to arrest the crack and offer relative resistance to its propagation as shown in AE and FESEM results. It is also possible that a higher suppression of grain growth in the sample with sawdust as pore formers which significantly minimizes free path for dislocation movement may have enhanced the hardness. Compressive strength for sample C (kaolin alone) was higher as compared to other samples. Compressive strength values recorded for samples A, B and C are 6.0, 6.3 and 9.2 MPa respectively. The gradient observed here is related to the maximum stress the samples absorbed before failure. This means that the yield strength for sample C is higher as it takes more time to completely fail as compared to the other samples. The elastic modulus (ratio of stress to strain) which measures the stiffness of the material shows that sample B has the highest resistance to elastic deformation and this can also be attributed to its tendency to relatively suppress crack propagation. The advantage of

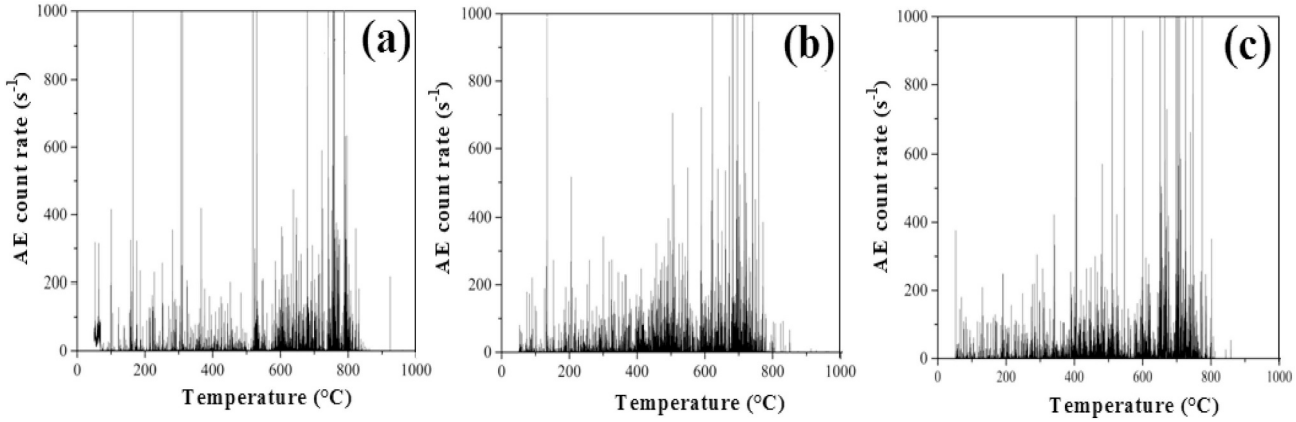

Fig. 3. AE signal intensity (a) Kaolin + styrofoam; (b) Kaolin + Sawdust; (c) Kaolin.

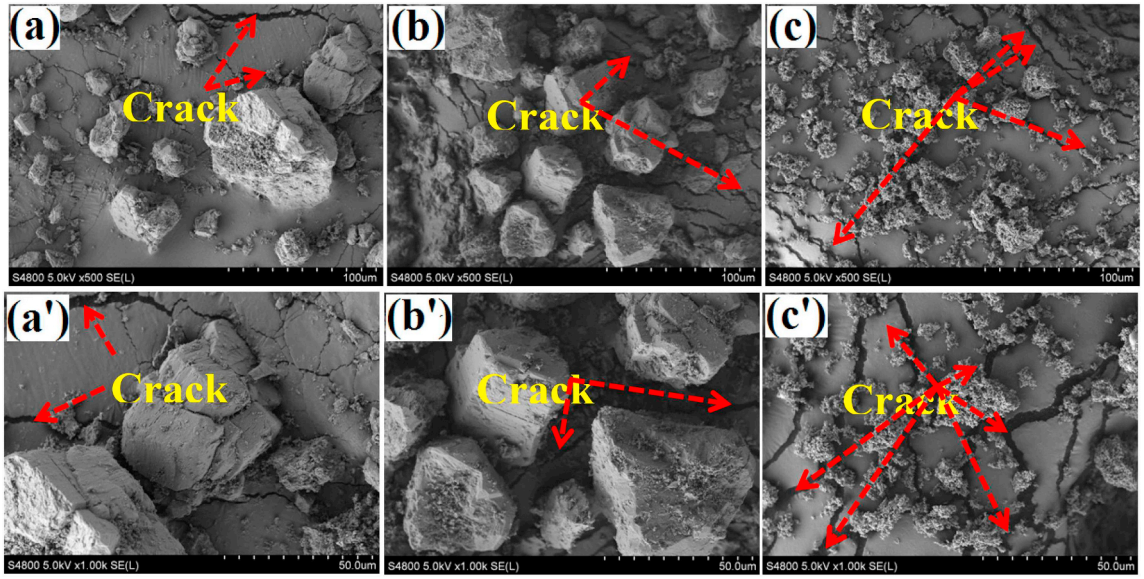

Fig. 4. FESEM images of (a) Kaolin + Styrofoam; (b)Kaolin + Sawdust; (c) Kaolin - at lower magnification (500×) and (a′) Kaolin + Styrofoam; (b′) Kaolin + Styrofoam (c′) Kaolin- at higher magnification (1000×).

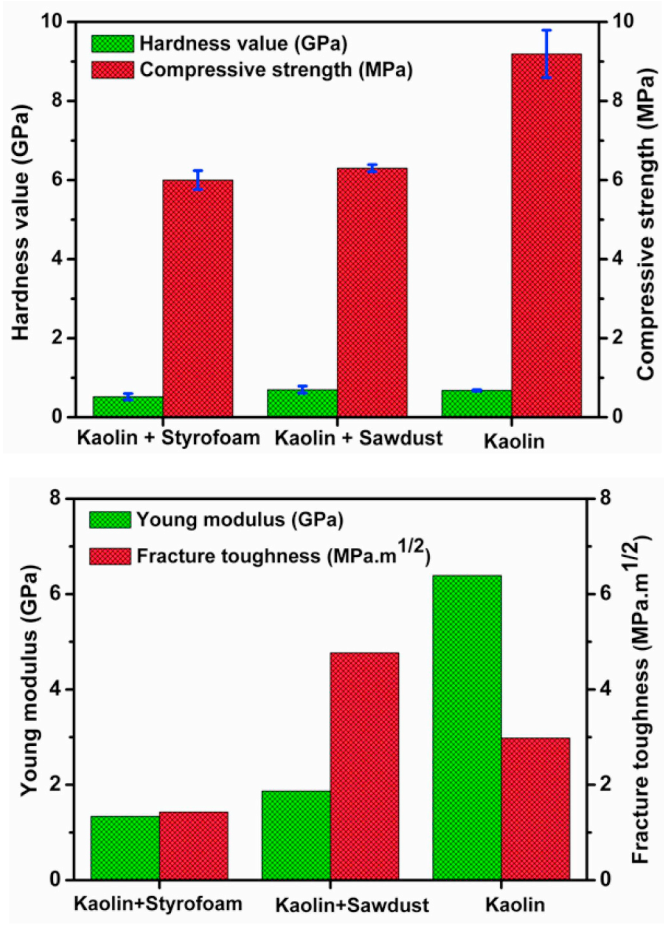

Fig. 5. Mechanical measurement data for the samples.

having a homogeneous distribution of pores on the mechanical strength in compression for all the samples tested in this study has already been noted for anisotropic porous ceramics processed by freeze-casting (Deville et al., 2015) or robocasting (Miranda et al., 2008). Enhanced fracture toughness values can be observed for sample B (4.77 MPa.m$^{1/2}$) compared to that of samples A and C with fracture toughness of 1.48 and 2.93 MPa.m$^{1/2}$ respectively. Again, the ability of sample B to provide relative resistance to crack propagation is the reason for its enhanced fracture toughness.

4. Conclusions

Kaolin-based ceramics with 2 different types of pore formers were prepared. After sintering, the apparent porosity of the samples was measured. The values confirmed the increased porosity of the samples with the sample prepared with styrofoam inclusion producing a porosity value of up to 47%. Acoustic emission (AE) activity was recorded in the cooling stage of firing. The AE counts appeared at 800 °C, where the compressive stresses between the different phases (particles with different coefficients of thermal expansion) led to an appearance of microcracks. By introducing porosity to the samples, the AE signals were less pronounced, especially for the sample with sawdust as pore former (Sample B), thus the microcracking was suppressed. Enhanced fracture toughness values observed for sample B (4.77 MPa.m$^{1/2}$) compared to that of samples A and C with fracture toughness of 1.48 and 2.93 MPa.m$^{1/2}$ was in line with AE measurement data and buttressed the fact that the enhanced fracture toughness noticed for sample B is due to its relative resistance to crack propagation. Mechanical measurements on samples used for physical, chemical and AE measurements prepared with the sintering protocol (1150 °C) as adopted in this study are necessary to further investigate the role of thermal match on the crack and mechanical behaviour of the porous ceramics.

Credit authorship contribution statement

David O. Obada: Conceptualization; Data curation; Formal analysis; Investigation; Methodology; Writing – original draft; Writing-review & editing

David Dodoo-Arhin: Supervision; Validation; Writing - original draft; Writing - review & editing.

Muhammad Dauda: Supervision

Fatai O. Anafi: Supervision

Abdulkarim S. Ahmed: Supervision

Olusegun A. Ajayi: Supervision

Stefan Csaki: Data curation; Writing - original draft; Writing - review & editing.

Naresh D. Bansod: Data curation; Writing - original draft; Writing - review & editing

Idris I. Kirim: Writing - review & editing

Omeiza J. Momoh: Writing - review & editing

Declaration of Competing Interest

We, the authors of the manuscript titled "Crack behaviour and mechanical properties of thermally treated kaolin based ceramics: The influence of pore generating agents" herby wish to declare that we have no conflict of interests.

References

Amlabu, B.A., Umaru, S., Dauda, M., Obada, D.O., Csaki, S., Bansod, N.D., Fasanya, O.O., 2019. Effect of ball milling time on the physical, thermal and fracture behaviour of 2MgO. $2Al_2O_3$. $5SiO_2$ precursors. Silicon 1–14.

Anderson, T.L., Anderson, T., 2005. Fracture Mechanics: Fundamentals and Applications. CRC press.

Azin, N.J., Camerucci, M.A., Cavalieri, A.L., 2005. Crystallisation of non-stoichiometric cordierite glasses. Ceram. Int. 31 (1), 189–195.

Aziz, M.H.A., Othman, M.H.D., Hashim, N.A., Rahman, M.A., Jaafar, J., Hubadillah, S.K., Tai, Z.S., 2019. Pretreated aluminium dross waste as a source of inexpensive alumina-spinel composite ceramic hollow fibre membrane for pretreatment of oily saline produced water. Ceram. Int. 45 (2), 2069–2078.

Biesheuvel, P.M., Verweij, H., 1999. Design of ceramic membrane supports: permeability, tensile strength and stress. J. Membr. Sci. 156 (1), 141–152.

Cannillo, V., Manfredini, T., Montorsi, M., Boccaccini, A.R., 2004. Use of numerical approaches to predict mechanical properties of brittle bodies containing controlled porosity. J. Mater. Sci. 39 (13), 4335–4337.

Capes, C.E., 2013. Particle Size Enlargement. Elsevier.

Chakrabarti, O.P., Ghosh, S., Mukerji, J., 1994. Influence of grain size, free silicon content and temperature on the strength and toughness of reaction-bonded silicon carbide. Ceram. Int. 20 (5), 283–286.

Chang, Q., Wang, Y., Cerneaux, S., Zhou, J.E., Zhang, X., Wang, X., Dong, Y., 2014. Preparation of microfiltration membrane supports using coarse alumina grains coated by nano TiO2 as raw materials. J. Eur. Ceram. Soc. 34 (16), 4355–4361.

Danwittayakul, S., Dutta, J., 2014. Controlled growth of zinc oxide microrods by hydrothermal process on porous ceramic supports for catalytic application. J. Alloys Compd. 586, 169–175.

Deville, S., Meille, S., Seuba, J., 2015. A meta-analysis of the mechanical properties of ice-templated ceramics and metals. Sci. Technol. Adv. Mater. 16 (4), 043501.

Dey, A., Kayal, N., Chakrabarti, O., Caldato, R.F., André, C.M., Innocentini, M.D., 2013. Permeability and nanoparticle filtration assessment of cordierite-bonded porous SiC ceramics. Ind. Eng. Chem. Res. 52 (51), 18362–18372.

Fukushima, M., Yoshizawa, Y.I., 2016. Fabrication and morphology control of highly porous mullite thermal insulators prepared by gelation freezing route. J. Eur. Ceram. Soc. 36 (12), 2947–2953.

Gonzalez-Velasco, J.R., Ferret, R., Lopez-Fonseca, R., Gutierrez-Ortiz, M.A., 2005. Influence of particle size distribution of precursor oxides on the synthesis of cordierite by solid-state reaction. Powder Technol. 153 (1), 34–42.

Green, D.J., 1998. An Introduction to the Mechanical Properties of Ceramics. Cambridge University Press.

Ismail, R.A., Almashhadani, N.J., Sadik, R.H., 2017. Preparation and properties of polystyrene incorporated with gold and silver nanoparticles for optoelectronic applications. Appl. Nanosci. 7 (3–4), 109–116.

Jang, B.K., Kim, S.Y., Han, I.S., Seo, D.W., Hong, K.S., Woo, S.K., Sakka, Y., 2010. Influence of uni and bi-modal SiC composition on mechanical properties and microstructure of reaction-bonded SiC ceramics. J. Ceram. Soc. Jpn. 118 (1383), 1028–1031.

Kim, H.W., Kim, H.E., Song, H., Ha, J., 1999. Effect of Oxidation on the Room-Temperature Flexural Strength of Reaction-Bonded Silicon Carbides. J. Am. Ceram. Soc. 82 (6), 1601–1604.

Knapek, M., Húlan, T., Minárik, P., Dobroň, P., Štubňa, I., Stráská, J., Chmelík, F., 2016. Study of microcracking in illite-based ceramics during firing. J. Eur. Ceram. Soc. 36 (1), 221–226.

Kouras, N., Harabi, A., Bouzerara, F., Foughali, L., Policicchio, A., Stelitano, S., ... Figoli, A., 2017. Macro-porous ceramic supports for membranes prepared from quartz sand and calcite mixtures. J. Eur. Ceram. Soc. 37 (9), 3159–3165.

Lenza, R.F.S., Vasconcelos, W.L., 2000. Synthesis and properties of microporous sol–gel silica membranes. J. Non-Cryst. Solids 273 (1–3), 164–169.

Masuda, H., Higashitani, K., Yoshida, H. (Eds.), 2006. Powder Technology: Fundamentals of Particles, Powder Beds, and Particle Generation. CRC press.

Mei, S., Yang, J., Ferreira, J.M.F., 2000. Microstructural evolution in sol–gel derived P2O5-doped cordierite powders. J. Eur. Ceram. Soc. 20 (12), 2191–2197.

Miranda, P., Pajares, A., Saiz, E., Tomsia, A.P., Guiberteau, F., 2008. Mechanical properties of calcium phosphate scaffolds fabricated by robocasting. J. Biom. Mater. Res. Part A 85 (1), 218–227.

Nandi, B.K., Uppaluri, R., Purkait, M.K., 2008. Preparation and characterization of low cost ceramic membranes for micro-filtration applications. Appl. Clay Sci. 42 (1–2), 102–110.

Nandi, B.K., Goswami, A., Purkait, M.K., 2009. Adsorption characteristics of brilliant green dye on kaolin. J. Hazard. Mater. 161 (1), 387–395.

Obada, D.O., Dodoo-Arhin, D., Dauda, M., Anafi, F.O., Ahmed, A.S., Ajayi, O.A., 2016a. Potentials of fabricating porous ceramic bodies from kaolin for catalytic substrate applications. Appl. Clay Sci. 132, 194–204.

Obada, D.O., Dodoo-Arhin, D., Dauda, M., Anafi, F.O., Ahmed, A.S., Ajayi, O.A., Samotu, I.A., 2016b. Effect of mechanical activation on mullite formation in an alumina-silica ceramics system at lower temperature. World J. Eng. 13 (4), 288–293.

Obada, D.O., Dodoo-Arhin, D., Dauda, M., Anafi, F.O., Ahmed, A.S., Ajayi, O.A., Samotu, I.A., 2016c. Physical and mechanical properties of porous kaolin based ceramics at different sintering temperatures. West Indian J. Eng. (1), 39.

Obada, D.O., Dodoo-Arhin, D., Dauda, M., Anafi, F.O., Ahmed, A.S., Ajayi, O.A., 2017a. Physico-mechanical and gas permeability characteristics of kaolin based ceramic membranes prepared with a new pore-forming agent. Appl. Clay Sci. 150, 175–183.

Obada, D.O., Dodoo-Arhin, D., Dauda, M., Anafi, F.O., Ahmed, A.S., Ajayi, O.A., 2017b. The impact of kaolin dehydroxylation on the porosity and mechanical integrity of kaolin based ceramics using different pore formers. Res. Phys. 7, 2718–2727.

Obada, D.O., Dodoo-Arhin, D., Dauda, M., Anafi, F.O., Ahmed, A.S., Ajayi, O.A., 2017c. Pressureless sintering and gas flux properties of porous ceramic membranes for gas applications. Res. Phys. 7, 3838–3846.

Obada, D.O., Dauda, E.T., Abifarin, J.K., Dodoo-Arhin, D., Bansod, N.D., 2020. Mechanical properties of natural hydroxyapatite using low cold compaction pressure: effect of sintering temperature. Mater. Chem. Phys., 122099. https://doi.org/10.1016/j.matchemphys.2019.122099.

Ohji, T., Fukushima, M., 2012. Macro-porous ceramics: processing and properties. Int. Mater. Rev. 57 (2), 115–131.

Rice, R.W., 1998. Porosity of Ceramics Marcel Dekker (New York).

Romanos, G.E., Steriotis, T.A., Kikkinides, E.S., Kanellopoulos, N.K., Kasselouri, V., Ramsay, J.D.F., ... Kallus, S., 2001. Innovative methods for preparation and testing of Al2O3 supported silicalite-1 membranes. J. Eur. Ceram. Soc. 21 (2), 119–126.

Scheffler, M., Colombo, P. (Eds.), 2006. Cellular Ceramics: Structure, Manufacturing, Properties and Applications. John Wiley & Sons.

Scholz, C.H., 2002. Earthquakes and Faulting.

Studart, A.R., Gonzenbach, U.T., Tervoort, E., Gauckler, L.J., 2006. Processing routes to macroporous ceramics: a review. J. Am. Ceram. Soc. 89 (6), 1771–1789.

Tancret, F., Bouler, J.M., Chamousset, J., Minois, L.M., 2006. Modelling the mechanical properties of microporous and macroporous biphasic calcium phosphate bioceramics. J. Eur. Ceram. Soc. 26 (16), 3647–3656.

Van Gestel, T., Vandecasteele, C., Buekenhoudt, A., Dotremont, C., Luyten, J., Leysen, R., ... Maes, G., 2002. Alumina and titania multilayer membranes for nanofiltration: preparation, characterization and chemical stability. J. Membr. Sci. 207 (1), 73–89.

Villanueva, H.H.S., de Mello, P.E.B., 2015. Heat transfer and pressure drop correlations for finned plate ceramic heat exchangers. Energy 88, 118–125.

Wang, S., Tian, J., Wang, Q., Zhao, Z., Cui, F., Li, G., 2019. Low-temperature sintered high-strength CuO doped ceramic hollow fiber membrane: Preparation, characterization and catalytic activity. J. Membr. Sci. 570, 333–342.

Wilhelm, M., Wruss, W., 2000. Influence of annealing on the mechanical properties of SiC–Si composites with sub-micron SiC microstructures. J. Eur. Ceram. Soc. 20 (8), 1205–1213.

Yang, M.Y., Wang, J.W., Li, L., Dong, B.B., Xin, X., Agathopoulos, S., 2019. Fabrication of low thermal conductivity yttrium silicate ceramic flat membrane for membrane distillation. J. Eur. Ceram. Soc. 39 (2–3), 442–448.

Zhu, L., Dong, Y., Hampshire, S., Cerneaux, S., Winnubst, L., 2015. Waste-to-resource preparation of a porous ceramic membrane support featuring elongated mullite whiskers with enhanced porosity and permeance. J. Eur. Ceram. Soc. 35 (2), 711–721.

Zuo, J., Chung, T.S., O'Brien, G.S., Kosar, W., 2017. Hydrophobic/hydrophilic PVDF/Ultem® dual-layer hollow fiber membranes with enhanced mechanical properties for vacuum membrane distillation. J. Membr. Sci. 523, 103–110.